Stability analyses of longitudinal rolls of poiseuille-Rayleigh- bénard flows in air-filled channels of finite transversal extension

S. Xin, Xavier Nicolas, P. Le Quere

NHT05/3976I

Stability analyses of longitudinal rolls of Poiseuille-Rayleigh-Bénard flows in air-filled channels of finite transversal extension

Shihe Xin[1,2], Xavier Nicolas[3] and Patrick Le Quéré[1]

[1] LIMSI-CNRS, BP 133, 91403 Orsay Cedex, France
[2] Dépt. de Physique, Univ. Paris Sud, 91405 Orsay Cedex
[3] LETEM, Univ. Marne-la-Vallée, 77454 Marne-la-Vallée Cedex 2, France

Tel : 33 1 69 85 80 33, Fax : 33 1 69 85 80 88, e-mail : xin@limsi.fr

Abstract: Time-stepping, steady-state solving and continuation methods are used to investigate the onset and stability of longitudinal rolls of Poiseuille-Rayleigh-Bénard flows in air-filled channels of finite transversal extension. In a channel of transversal aspect ratio 10, three solution branches of steady longitudinal rolls are discovered. Those with respectively 9 and 10 rolls are linked to supercritical pitchfork bifurcations of the base flow while that with 11 rolls seems to be an isolated branch. All three branches of longitudinal rolls are found to be unstable with respect to wavy oscillatory perturbations and nonlinear studies show that the coresponding Hopf bifurcations are supercritical.

Key words: linear stability analysis, longitudinal rolls, Poiseuille-Rayleigh-Bénard flows.

Nomenclature

B	transversal aspect ratio ($= L/H$)
C	constant
H	channel height
J	Jacobian
k	longitudinal wave number
L	channel width
N	cut-off degree of Chebyshev polynomials
P	pressure deviation
p	pressure perturbation
Pr	Prandtl number ($= \nu/\kappa = 0.71$)
Ra	Rayleigh number ($= g\beta(T_h - T_c)H^3/(\nu\kappa)$)
Re	Reynolds number $\left(= U_m^{2d}H/\nu\right)$
T	temperature
t	time
U, V, W	longitudinal, transversal and vertical velocity components
u, v, w	longitudinal, transversal and vertical velocity perturbations
x	eigen-vector of the Jacobian
x, y, z	Cartesian coordinates

Greek symbols

β	coefficient of volumetric thermal expansion
$\Delta T = T_h - T_c$	temperature difference
κ	thermal diffusivity
ν	kinematic viscosity
ρ	density
σ, ω	real and imaginary parts of an eigen-value
τ	constant
Θ	reduced temperature
θ	perturbations of reduced temperature

Super and subscripts

0	related to the reference temperature
$2d$	two-dimensional
$3d$	three-dimensional
c	critical or cold
e	entrance
h	hot
m	mean
ref	reference
t	total

1 Introduction

Poiseuille-Rayleigh-Bénard (PRB) flows, mixed convection flows in a horizontal channel heated from below, enjoy increasing attention of fluid and thermal sciences communities

because of their applications in chemical vapor deposition (CVD) of solid layers (see [11, 16] among others for CVD and [19] for a general review of PRB flows). In PRB problem, the combination of Bénard cells (rolls) with a Poiseuille flow gives rise to, at relatively low Reynolds and Rayleigh numbers, very complex flow structures ranging from time-dependent transversal rolls, steady longitudinal rolls to mixed rolls. Time-dependent transversal rolls (rotating in the vertical plane of two-dimensional Poiseuille flow) occur at very low Reynolds number and have been extensively studied in the past. However, in cold wall thermal rectangular reactors at atmospheric pressure, operating conditions generally result in steady longitudinal rolls which prevent from a uniform deposit. Understanding, manipulating and controlling steady longitudinal rolls are therefore important and there need further numerical and experimental investigations of steady longitudinal rolls.

As both time-dependent transversal rolls and steady longitudinal rolls can set up from the well-known simple 2D base flow—linear conduction profile of temperature combined with streamwise Poiseuille flow—many linear and weakly nonlinear stability analyses of this simple base flow have been conducted in the past in channels of both infinite and finite transversal extension [5, 10, 12, 16, 18, 20]. In a channel of infinite transversal extension, longitudinal rolls set up for Rayleigh number above 1708. Channel lateral confinement delays the onset of steady longitudinal rolls, ie, critical Rayleigh numbers increase with decreasing channel transversal extension. At small Reynolds number, time-dependent transversal rolls will set up below neutral curves of steady longitudinal rolls and the corresponding critical Rayleigh numbers depend on both Prandtl number and the channel transversal extension.

It is interesting to note that, in a laterally confined channel, time-dependent transversal rolls result in three-dimensional time-dependent flows while steady longitudinal rolls, despite the velocity field of 3 non-trivial components, give rise to steady two-dimensional flows as there is flow translation in the streamwise direction. This leads naturally to the conclusion that the stability of steady longitudinal rolls is a stability problem of two-dimensional base flows with respect to three-dimensional perturbations. Due to the fact that solutions of steady longitudinal rolls are not analytical, Clever and Busse [9] performed to our knowledge the only linear stability analysis of steady longitudinal rolls in a channel of infinite transversal extension while Kato and Fujimura [13] the only linear stability analysis of steady longitudinal rolls in a square channel. They showed the wavy instability of longitudinal rolls observed in the experiments of Avsec [1] and Avsec & Luntz [2]. In CVD processes, wavy oscillatory instability of longitudinal rolls giving rise to time-dependent flows would reult in a more uniform deposit and is of practical interest. The present work is thus mainly motivated by doing stability analyses of steady longitudinal rolls—two-dimensional convective PRB flows in channels of finite transversal extension.

In fact, tremendous progress has been made in numerical methods of steady-state solving and linear stability analysis during the last fifteen years. Steady-state solving consists in obtaining both stable and unstable numerical solutions satisfying the steady Navier-Stokes equations. These discrete solutions are then used as base flow to linearize the unsteady Navier-Stokes equations and their stability is deduced by studying the linearized unsteady Navier-Stokes equations. Amongst the methods available, the method proposed by Mamun and Tuckerman [17] is very effective and has been applied successfully to a differentially heated circular cavity [26] and extended to investigate stability of a two-dimensional base flow with respect to three-dimensional perturbations [24]. The method proposed in [17] makes use of a first-order time-stepping scheme of the unsteady Navier-Stokes equations, computes the steady-state solutions through Newton's iteration and avoids explicit construction of the Jacobian by using Stokes preconditioning. Linear stability analysis can be done by using the same first-order time-stepping scheme and Arnoldi's method because this scheme with small time step results in an approximate exponentiation of the Jacobian. The extension brought in [24] consists of Stokes preconditioning of the eigen-system, continuation method and coupling of steady-state solving and the eigen-system. More details on the method and its extension can be found in [17, 24]. Note that for the cases studied previously in [24, 26] the base velocity component normal to the two-dimensional plane in which the base flow evolves is equal to zero. This makes the real and imaginary parts of perturbations independent and allows to work on only one part of the perturbations. For longitudinal rolls in PRB flows, however, streamwise component of the base velocity field couples the real and imaginary parts of perturbations and one has to work on both the real and imaginary parts. The second motivation of the present work is to extend the methods used in [24, 26] to the general case in which the base flow has three non-trivial velocity components.

Although linear stability analysis yields interesting results and remains sometimes difficult to perform, it leads only to partial conclusions: for example after doing linear stability analysis one knows the threshold of the base flow stability and the type of bifurcation (pitchfork, transcritical or Hopf) that the base flow will undergo, but one can not tell whether the bifurcation is supercritical and whether the bifurcated solution will remain stable. This suggests that both linear stability analysis and nonlinear analysis should be performed together in order to draw a full conclusion on a bifurcation. In the present work, whenever is possible, nonlinear time-stepping computations, guided by results of linear stability analysis, are performed to provide further information.

As PRB flows in channels depend on Reynolds number (Re), Rayleigh number (Ra), Prandtl number (Pr) and channel width/height aspect ratio (B), we focus, in the present study, on an air-filled channel of width/height aspect ratio 10. The PRB flows considered will thus only depend on Reynolds number and Rayleigh number. Furthermore, in order to assess the validity of the newly developed code, stability analysis was performed for the

onset of longitudinal rolls and results were compared to those available in the literature. In next section we present the physical problem of interest, its mathematical formulation and the numerical procedures used. Numerical results will be discussed before giving the final concluding remarks.

2 Physical problem, mathematical formulations and numerical methods

2.1 Physical problem

We consider a rectangular channel of infinite length as illustrated in Figure 1. The width/height aspect ratio, B, is fixed to 10, the channel is filled with air ($Pr = 0.71$) and air flow is driven by a mean pressure gradient normal to y–z plane in x direction. The channel vertical walls are thermally insulated (adiabatic), its bottom wall is heated at a constant temperature, T_h, and its top wall is cooled at another constant temperature, T_c. We are interested in air flows resulting from competition between the pressure gradient and the buoyancy in the channel.

The trivial flow in the channel occurs for small Ra: Poiseuille flow in x direction is associated with a linear vertical temperature distribution. For Ra larger than a critical value, Bénard cells will set up. If Bénard cells are in line with y-axis, one observes transversal cells. This happens only for very small Re and wiil not be considered here. We only consider the cases in which Bénard cells are parallel to x direction: the resulted flow in the form of longitudinal rolls is steady and independent of x. Particular attention is paid to stability analysis of longitudinal rolls.

2.2 Governing equations

Let us consider that air filling the channel is a Newtonian viscous fluid of thermal diffusivity κ, kinematic viscosity ν and thermal expansion coefficient β. We are interested in two dimensional flow solutions in y–z plane and in their stability characteristics with respect to both two dimensional and three dimensional perturbations. We assume that the two-dimensional base flow in the channel is governed by the steady Navier-Stokes equations under Boussinesq approximation which consists of assuming that, in the buoyancy term, the fluid density is expanded as $\rho(T) = \rho_0(T_0)[1 - \beta(T - T_0)]$.

Using the temperature difference $\Delta T = T_h - T_c$, $T_0 = T_c$ and the channel height, H, as reference length, we define Rayleigh number as $Ra = g\beta\Delta T H^3/(\nu\kappa)$ and the reduced temperature as $\Theta = (T - T_0)/\Delta T$. Although the driving forces of PRB flows—mean pressure gradient and buoyancy—result in two different velocity scales, it is still convenient to work with the scale of two-dimensional Poiseuille flow. In $x-z$ plane any

constant pressure gradient in x direction results in a parabolic x-velocity profile and one can use the mean velocity, U_m^{2d}, as reference velocity and define Reynolds number as $Re = U_m^{2d}H/\nu$. This leads to a dimensionless velocity distribution of $6z(1-z)$ and a mean dimensionless pressure gradient of $-12/Re$. In the present study, we continue with U_m^{2d} as reference velocity, but note that the dimensionless mean velocity, U_m^{3d}, in a channel of finite transversal extension is no longer equal to 1: U_m^{3d} increases with B and converges to 1 for $B \to \infty$, for some values of B the relationship between U_m^{2d} and U_m^{3d} is given in [20]. The corresponding reference pressure and reference time are therefore $P_{\text{ref}} = \rho_0(U_m^{2d})^2$ and $t_{\text{ref}} = H/U_m^{2d}$. The steady Navier-Stokes equations governing longitudinal rolls read in dimensionless form:

$$
\begin{aligned}
0 &= \frac{\partial V}{\partial y} + \frac{\partial W}{\partial z} \\
0 &= \frac{12}{Re} + \frac{1}{Re}(\frac{\partial^2}{\partial y^2} + \frac{\partial^2}{\partial z^2})U - V\frac{\partial U}{\partial y} - W\frac{\partial U}{\partial z} \\
0 &= -\frac{\partial P}{\partial y} + \frac{1}{Re}(\frac{\partial^2}{\partial y^2} + \frac{\partial^2}{\partial z^2})V - V\frac{\partial V}{\partial y} - W\frac{\partial V}{\partial z} \\
0 &= -\frac{\partial P}{\partial z} + \frac{1}{Re}(\frac{\partial^2}{\partial y^2} + \frac{\partial^2}{\partial z^2})W + \frac{Ra}{Pr\,Re^2}\Theta - V\frac{\partial W}{\partial y} - W\frac{\partial W}{\partial z} \\
0 &= \frac{1}{PrRe}(\frac{\partial^2}{\partial y^2} + \frac{\partial^2}{\partial z^2})\Theta - V\frac{\partial \Theta}{\partial y} - W\frac{\partial \Theta}{\partial z}
\end{aligned}
\tag{1}
$$

The boundary conditions are no-slip for velocity, $\Theta(y,0) = 1$, $\Theta(y,1) = 0$ and adiabatic on the vertical walls, i.e. $\frac{\partial \Theta}{\partial y}|_{y=0,B} = 0$. Note that in the above equations P does not take into account the mean pressure gradient in the x direction.

Stability of the base flow (U, V, W, Θ) with respect to 3D periodic disturbances is governed by the following linearized unsteady Navier-Stokes equations :

$$
\begin{aligned}
0 &= \mathbf{i}k\,u + \frac{\partial v}{\partial y} + \frac{\partial w}{\partial z} \\
\frac{\partial u}{\partial t} &= -\mathbf{i}k\,p + \frac{1}{Re}(\frac{\partial^2}{\partial y^2} + \frac{\partial^2}{\partial z^2} - k^2)u - \mathbf{i}k\,uU - V\frac{\partial u}{\partial y} - W\frac{\partial u}{\partial z} - v\frac{\partial U}{\partial y} - w\frac{\partial U}{\partial z} \\
\frac{\partial v}{\partial t} &= -\frac{\partial p}{\partial y} + \frac{1}{Re}(\frac{\partial^2}{\partial y^2} + \frac{\partial^2}{\partial z^2} - k^2)v - \mathbf{i}k\,vU - V\frac{\partial v}{\partial y} - W\frac{\partial v}{\partial z} - v\frac{\partial V}{\partial y} - w\frac{\partial V}{\partial z} \\
\frac{\partial w}{\partial t} &= -\frac{\partial p}{\partial z} + \frac{1}{Re}(\frac{\partial^2}{\partial y^2} + \frac{\partial^2}{\partial z^2} - k^2)w + \frac{Ra\theta}{Pr\,Re^2} - \mathbf{i}k\,wU - V\frac{\partial w}{\partial y} - W\frac{\partial w}{\partial z} - v\frac{\partial W}{\partial y} - w\frac{\partial W}{\partial z} \\
\frac{\partial \theta}{\partial t} &= \frac{1}{PrRe}(\frac{\partial^2}{\partial y^2} + \frac{\partial^2}{\partial z^2} - k^2)\theta - \mathbf{i}k\,\theta U - V\frac{\partial \theta}{\partial y} - W\frac{\partial \theta}{\partial z} - v\frac{\partial \Theta}{\partial y} - w\frac{\partial \Theta}{\partial z}
\end{aligned}
\tag{2}
$$

Three dimensional perturbations are of the form $[u, v, w, p, \theta](y, z, t)\exp(\mathbf{i}k\,x)$ where k is the wave number in x direction. Boundary conditions of Equations (2) are homogeneous and of the same type as for Equations (1).

When $k = 0$, perturbations are only two dimensional in the sense that they depend only on y and z and their real and imaginary parts are decoupled. It corresponds to the case of the onset of longitudinal rolls. In this particular case, Equations (1) are reduced to:

$$\begin{aligned} V = W &= 0 \\ \frac{12}{Re} + \frac{1}{Re}(\frac{\partial^2}{\partial y^2} + \frac{\partial^2}{\partial z^2})U &= 0 \\ \Theta &= 1 - z \end{aligned} \tag{3}$$

and Equations (2) to:

$$\begin{aligned} 0 &= \frac{\partial v}{\partial y} + \frac{\partial w}{\partial z} \\ \frac{\partial u}{\partial t} &= \frac{1}{Re}(\frac{\partial^2}{\partial y^2} + \frac{\partial^2}{\partial z^2})u - v\frac{\partial U}{\partial y} - w\frac{\partial U}{\partial z} \\ \frac{\partial v}{\partial t} &= -\frac{\partial p}{\partial y} + \frac{1}{Re}(\frac{\partial^2}{\partial y^2} + \frac{\partial^2}{\partial z^2})v \\ \frac{\partial w}{\partial t} &= -\frac{\partial p}{\partial z} + \frac{1}{Re}(\frac{\partial^2}{\partial y^2} + \frac{\partial^2}{\partial z^2})w + \frac{Ra}{Pr\,Re^2}\theta \\ \frac{\partial \theta}{\partial t} &= \frac{1}{PrRe}(\frac{\partial^2}{\partial y^2} + \frac{\partial^2}{\partial z^2})\theta + w \end{aligned} \tag{4}$$

Solutions of Equations (3) possess the four following symmetries: translation symmetry in time ($t \to t + \tau$), translation symmetry in x ($x \to x + C$), reflection symmetry in y ($y \to B - y$) and centro-symmetry ($(y, z) \to (B - y, 1 - z)$), ie,

Translation symmetry in time : $(U, V, W, \Theta)(x, y, z, t) = (U, V, W, \Theta)(x, y, z, t + \tau)$

Translation symmetry in x : $(U, V, W, \Theta)(x, y, z, t) = (U, V, W, \Theta)(x + C, y, z, t)$

Reflection symmetry in y : $(U, V, W, \Theta)(x, y, z, t) = (U, -V, W, \Theta)(x, B - y, z, t)$

Centro-symmetry : $(U, V, W, \Theta)(x, y, z, t) = (U, -V, -W, -\Theta)(x, B - y, 1 - z, t)$

Two-dimensional perturbations governed by Equations (4) will break either the reflection symmetry in y or the centro-symmetry, ie, given the boundary conditions, Equations (1) governing longitudinal rolls admit either reflection symmetry in y and translation symmetries both in time and in x or centro-symmetry and translation symmetries both in time and in x. Any wavy instability whose perturbations are governed by Equations (2) breaks the translation symmetries in time and in x and will beak at the same time the other symmetry admitted by Equations (1).

Nonlinear behavior of the unstable modes of Equations (3) is governed by Equations (1) in unsteady form. While wave instability dynamics is governed by the following

full three-dimensional unsteady Navier-Stokes equations:

$$\begin{aligned} 0 &= \frac{\partial U}{\partial x} + \frac{\partial V}{\partial y} + \frac{\partial W}{\partial z} \\ \frac{\partial U}{\partial t} + U\frac{\partial U}{\partial x} + V\frac{\partial U}{\partial y} + W\frac{\partial U}{\partial z} &= \frac{12}{Re} - \frac{\partial P}{\partial x} + \frac{1}{Re}(\frac{\partial^2}{\partial x^2} + \frac{\partial^2}{\partial y^2} + \frac{\partial^2}{\partial z^2})U \\ \frac{\partial V}{\partial t} + U\frac{\partial V}{\partial x} + V\frac{\partial V}{\partial y} + W\frac{\partial V}{\partial z} &= -\frac{\partial P}{\partial y} + \frac{1}{Re}(\frac{\partial^2}{\partial x^2} + \frac{\partial^2}{\partial y^2} + \frac{\partial^2}{\partial z^2})V \\ \frac{\partial W}{\partial t} + U\frac{\partial W}{\partial x} + V\frac{\partial W}{\partial y} + W\frac{\partial W}{\partial z} &= -\frac{\partial P}{\partial z} + \frac{1}{Re}(\frac{\partial^2}{\partial x^2} + \frac{\partial^2}{\partial y^2} + \frac{\partial^2}{\partial z^2})W + \frac{Ra}{Re^2}\Theta \\ \frac{\partial \Theta}{\partial t} + U\frac{\partial \Theta}{\partial x} + V\frac{\partial \Theta}{\partial y} + W\frac{\partial \Theta}{\partial z} &= \frac{1}{PrRe}(\frac{\partial^2}{\partial x^2} + \frac{\partial^2}{\partial y^2} + \frac{\partial^2}{\partial z^2})\Theta \end{aligned} \tag{5}$$

Periodic conditions are prescribed in the x direction and the domain size in x is determined by the critical wave number k_c through $2\pi/k_c$.

2.3 Numerical methods

Linear stability analysis needs codes doing steady-state solving (base solution), searching eigenvalues through Arnoldi's method and determining critical points by continuation method. Nonlinear behavior of the unstable modes needs time-stepping codes. A full understanding of the critical modes in PRB flows demands a complete set of numerical tools: a two-dimensional code for steady-state solving; a two-dimensional code integrating Equations (4) and doing Arnoldi's method; a quasi-three-dimensional code integrating Equations (2) and doing Arnoldi's method; a code doing continuation to the 2D unstable modes governed by Equations (4); another code doing continuation to the 3D unstable modes governed by Equations (2); a 2D time-stepping code integrating the unsteady form of Equations (2) and a 3D time-stepping code solving Equations (5). A brief description of the numerical methods used are given in the following and references will be provided for more details.

Time-stepping codes

Time-stepping codes are the basis of steady-state solving and linear stability analysis through Arnoldi's method and continuation method. They combine a second-order backward differencing discretization BDF2 with a second-order Adams Bashforth extrapolation for the convective terms. This time scheme results in Helmholtz equations for velocity components and temperature. Spectral Chebyshev collocation methods are used for spatial discretization in $y - z$ plane and direct Uzawa method ensures fluid incompressibility (velocity-pressure coupling). Details of spectral methods and Uzawa method can be found in [3, 4]. For the full 3D equations (5), Fourier Galerkin method is used for discretization in the x direction. In this case velocity-pressure coupling is dealt with projection method due to the fact that Uzawa operator has a very large dimension. The 3D time-stepping code is described in [25].

In both the 2D and 3D codes, the resulting Helmholtz equations for the unknowns are solved by a direct method based on full diagonalization of the second-order partial derivatives.

Steady-state solving

Usually, time-stepping codes are only capable of providing stable steady-state solutions. In order to obtain both stable and unstable steady-state solutions, one should resort to Newton's iteration. The interesting idea proposed in [17, 23] is to take advantage of the existing time-stepping schemes for the unsteady Navier-Stokes equations and use a first-order semi-implicit time scheme (implicit treatment for diffusion terms and explicit for the remaining terms). The difference between solutions at two consecutive time steps has the same root as the steady-state Navier-Stokes equations and is equal to the residual of preconditioned steady-state Navier-Stokes equations. The same reasoning applied to the linearized unsteady Navier-Stokes equations allows to compute an action of the preconditioned Jacobian on a vector and to do Newton's iteration by using matrix-free methods as GMRes or BCG-Stab. Explicit construction of the Jacobian is thus avoided. This method has been found to be very efficient for large time step with which the time-stepping scheme reduces to the Stokes operator which can be viewed as a preconditioner of the steady state equations. More details of the methods can be found in [17, 23] and applications to natural convection flows in [24, 25].

Linear stability analysis

When the same first-order semi-implicit time scheme is applied to the linearized unsteady Navier-Stokes equations with very small time step, solutions at one time step is an application of approximate exponentiation of the Jacobian to those at the previous step. This time scheme transforms therefore the leading eigenvalues of the Jacobian with the largest real parts into those of maximum modulus and Arnoldi's method can be used to calculate them. As accurate eigenvalues impose a very small time step, a large number of time steps are usually needed.

Improving accuracy and efficiency of the computations has been done in [24, 25]. The idea is to use the results of Arnoldi's method as initial estimates of the eigenmodes and work, by combining a continuation technique [14] with Stokes preconditioning, on $Jx = (\sigma + \mathrm{i}\omega)x$ where $(\sigma + \mathrm{i}\omega)$ is an eigenvalue of the Jacobian J and x is the corresponding eigenfunction containing (u, v, w, θ). The results obtained will satisfy the discrete equations, $Jx = (\sigma + \mathrm{i}\omega)x$, to round-off level.

Solving the eigen-system using continuation technique, Stokes preconditioning and Newton's iteration has also been coupled with steady-state solving and a secant method for searching roots of $\sigma = 0$. This allows for an accurate computation of critical values. Embeding this coupling in a do-loop of wave number will enable to construct neutral curves versus wave number.

Note that, if J is real, its size is equal to 4 times the grid points. In case of a complex

Jacobian, its size is equal to 8 times the grid points. For $B = 10$ we used for example a spatial resolution of 200×30 (a grid of 201×31 points), the discrete Jacobian is of size 24924 or 49848 and using an iterative method to solve the eigen-system is completely justified.

Nonlinear analysis

As time-stepping codes are available, it is straightforward to do nonlinear analysis by integrating the unsteady Navier-Stokes equations. Time evolutions of perturbations will indicate whether a bifurcation is supercritical and whether solutions after bifurcation are stable. If there are several unstable modes and their critical values are close, one needs to start computations with appropriate perturbations in order to study the unstable modes one by one. A straightforward way is to perturb the base solution using the eigenfunction of the unstable mode. This is particularly the case of $B = 10$ as there are multiple solutions of longitudinal rolls.

Summary and remarks

In summary a typical numerical procedure to study 3D periodic perturbations is the following: for a given set of parameters (Re, Ra, Pr, B, for example), 2D steady-state solving is used first to obtain base solutions (solving Equations (3) for example); Equations (4) are then integrated in order to calculate the leading eigen-modes of the Jacobian using Arnoldi's method; for each leading mode estimated by Arnoldi's method, the eigen-system coupled with steady-state solving and a secant method are then solved to determine the critical point and construct neutral curves; a 3D time-stepping code is finally used to investigate nonlinear behavior of the unstable modes.

Concerning wavy instability of longitudinal rolls, the terms $\mathrm{i}kU(u, v, w, \theta)$ in Equations (2) couple the real and imaginary parts of the perturbations. This requires to work with both the real and imaginary parts and leads to doubling the dimension of the Jacobian. In this sense, stability of longitudinal rolls of PRB flows is the most complicated case of linear stability analysis in Cartesian coordinates and it is thus interesting to show the feasibility of such analysis.

Note also that longitudinal rolls are Bénard cells and have a regular distribution in y direction. They are generally convenient for a uniform grid but problematic for Chebyshev collocation methods. In fact spectral Chebyshev methods use Gauss-Lobatto collocation points which are fine near the domain ends and coarse near the domain center, *ie* the grid size is $\mathcal{O}(\pi^2/N^2)$ near the domain ends and $\mathcal{O}(\pi/N)$ near the domain center with N the cut-off degree of Chebyshev polynomials. A good approximation of the Bénard cells at the channel center requires higher spatial resolution, *ie* bigger N, especially in the cases of large B. This is why we have had to check the numerical results with a spatial resolution of 200×30 in the case of $B = 10$.

3 Numerical results and discussions

The validity of the newly developed code is assessed by computing the critical Rayleigh numbers corresponding to the onset of longitudinal rolls for $B = 3$ and 4 as they were provided earlier by Nicolas *et al* [20]. The onset of longitudinal rolls at $B = 10$ is studied in detail as one can expect multiple solutions with increasing B and multiple solutions of longitudinal rolls would complicate the subsequent linear stability analysis.

3.1 Onset of longitudinal rolls: linear stability analysis

The onset of longitudinal rolls in channels of finite transversal extension corresponds to pitchfork bifurcations, it does not depend on Re nor on Pr and it was investigated in detail for B ranging from 0.1 to 5.4 in [15, 20] and from 1 to 4 in [12]. Critical Rayleigh numbers obtained for $B = 3$ and 4 are listed in Table 1 together with spatial resolutions used: they agree well with those provided in [15, 20] and perfectly with those of Kato and Fujimura [12]. We checked grid independence of the present results for $B = 4$ as is shown in Table 1. The slight differences between the present results and those in [15, 20] may come from the ilimited spatial resolutions used in [15, 20] (Table 1). Kato and Fujimura [12] used more polynomial modes and obtained grid independent results. The critical modes for $B = 3$ and 4 consist of respectively 3 and 4 rolls.

Early studies [22, 20] showed the transition in number of rolls in flow structure. This seems to indicate that above Ra_c shown in Table 1 there should be other unstable modes characterized by different roll numbers. For $B = 3$, we found another unstable mode of 2 rolls with $Ra_c = 2030.8094$ and, for $B = 4$, another mode of 3 rolls becomes unstable at $Ra_c = 1876.0997$.

The case of $B = 10$ was investigated using a spatial resolution of 140×30: several modes were found out to become unstable in a small range of Ra and the corresponding Ra_c are shown in Table 2. Spatial structures of the unstable modes are displayed in Figure 2: one distinguishes the first two regular modes (Modes 1 and 2) from two other irregular modes (Modes 3 and 4). The regular Modes 1 and 2 contain respectively 10 and 9 Bénard cells of almost equal size and possess respectively the reflection symmetry in y and the centro-symmetry. The irregular Modes 3 and 4 contain respectively 11 and 12 cells and possess respectively the centro-symmetry and the reflection symmetry in y. Although the irregular modes seem to be curious, both their critical values and spatial structures are confirmed by a higher spatial resolution of 200×30. Note that the linear modes leading to longitudinal rolls in PRB flows are identical to those of Rayleigh-Bénard convection, unfortunately no relevant results on Rayleigh-Bénard convection in high aspect ratio box have been found in the literature. Further studies should be done for different aspect ratios in order to understand the behavior of each mode in terms of aspect ratio B.

3.2 Onset of longitudinal rolls: nonlinear behavior

Although the critical values and the linear unstable modes characterizing the onset of longitudinal rolls are independent of Pr and Re, their nonlinear behavior does depend on them. In the following we use air as the working fluid ($Pr = 0.71$) and we fix Reynolds number to $Re = 200$ and the aspect ratio to $B = 10$. All the 2D results presented hereafter are obtained with a spatial resolution of 200×30.

The nonlinear behavior of the onset of longitudinal rolls can only be observed by using a time-stepping code which integrates the 2D unsteady Boussinesq equations. These computations not only reveal the supercritical or sub-critical nature of the corresponding pitchfork bifurcation but also provide steady-state base solutions for analysis of wavy instabilities. In practice time-stepping is used only to reveal the nature of the pitchfork bifurcation and steady-state solving is used to produce the base solutions once a steady-state solution after bifurcation is obtained by time-stepping. As the linear unstable modes shown in Table 2 and Figure 2 occur in a very small range of Rayleigh number, multiple steady-state solutions are likely. The initial conditions used in the present work are the base solutions perturbed by the corresponding linear unstable modes.

Time-stepping computations performed at $Ra = 2000$ for Modes 1 and 2 revealed that the corresponding pitchfork bifurcations are supercritical, which is also confirmed by the fact that flow structures of the final steady-state (Figure 3) are very similar to the linear unstable Modes 1 and 2. What happened for Modes 3 and 4 is curious: at $Ra = 2000$ starting with the base solutions perturbed respectively by Modes 3 and 4, we obtained finally steady-state solutions possessing respectively 9 and 10 regular Bénard cells, *ie* those displayed in Figure 3; at $Ra = 2400$ Mode 3 led to a steady-state solution of 11 regular Bénard cells while Mode 4 always led to a 10 cell solution. In order to understand the nonlinear behavior of solutions with 11 Bénard cells, steady-state solving was used and combined with quadratic extrapolation if necessary to investigate higher and lower Rayleigh numbers. For lower Rayleigh numbers a turning point was located at $Ra = 2120$ and unstable steady-state solutions are obtained after the turning point for higher Rayleigh numbers. The details are illustrated in Figure 4. Compared to solutions on the stable upper branch, those on the lower unstable branch have two smaller weakened cells at the channel lateral ends and strengthened central cells. Computations were realized up to $Ra = 15000$ beyond the range of Rayleigh number shown in Figure 4 and both branches subsist. It seems to indicate that solutions with 11 longitudinal rolls are only an isolated branch which is not connected to the base solutions governed by Equations (3).

Concerning the onset of longitudinal rolls, the nonlinear studies reveal up to now three different branches of stable steady-state solutions with respectively 9, 10 and 11 Bénard cells. In the following we consider them as base solutions and study their stability with respect to 3D periodic perturbations although the existence of other branches of

steady-state solutions can not be excluded.

3.3 Onset of wavy instability: linear stability analysis

For each branch of stable longitudinal rolls, steady-state solving yields solutions for different Rayleigh numbers and, for each longitudinal wave number k, approximate exponentiation of the Jacobien combined with Arnoldi's methods indicates stability of the base solution. Continuation method using Newton's iteration applied to the preconditioned eigen-system combined with steady-state solving and secant method yields the critical values corresponding to the wave number k investigated. A loop over k builds up the neutral curves.

Different test-and-error computations performed for the solution branch of 10 Bénard cells indicate that they become unstable to 3D oscillatory perturbations, through a Hopf bifurcation. Figure 5 shows the neutral curve and the corresponding critical angular frequency: the neutral curve has a minimum at approximately $k = 0.8$ and the critical angular frequency is a linear function of the wave number k ($\omega_c = 1.01k$). The corresponding critical values are respectively $k_c = 0.818 \pm 0.001$, $Ra_c = 3414.62 \pm 0.03$ and $\omega_c = 0.83103$ (Table 3). Eigen-temperature of the critical mode is displayed in Figure 6. As can be seen, the unstable mode breaks both the translation symmetry in x and the reflection symmetry in y. The critical mode is concentrated on the central part of the channel and damped by the lateral confinement.

Similar results obtained for the solution branches with 9 and 11 Bénard cells are shown in Figures 7, 8, 9 and 10. The results obtained are similar to those shown in Figures 5 and 6: minima of Rayleigh number for k about 0.8 and critical modes breaking both the the translation symmetry in x and the centro-symmetry in the vertical $y-z$ plane. Table 3 details the critical values and shows that it is the branch of 11 Bénard cells that has the lowest critical Rayleigh number. (The corresponding critical point is displayed in Figure 4.)

Compared to the study on a channel of infinite transversal extension realized by Clever and Busse [9], the lateral confinement introduced by finite transversal extension first makes the neutral curves to take usual forms. In fact in a channel of infinite transversal extension, the neutral curves have minima at $k = 0$ and the critical angular frequency is linear with k and equal to zero at $k = 0$. The lateral confinement shifts the critical points to $k \neq 0$ with $\omega_c \neq 0$ although the linear relationship between k and ω_c subsist. The lateral confinement slightly delays the onset of steady longitudinal rolls and strongly the onset of wavy oscillatory instability. In other words, it increases the corresponding critical Rayleigh numbers. This is due to the fact that the confinement damps not only longitudinal rolls but also the critical modes near the channel lateral ends. Although there are choices for transversal wave length of the longitudinal rolls

at supercritical Rayleigh numbers in a channel of infinite transversal extension, Clever and Busse [9] used mainly, in their analyses for $Pr = 0.7$, the critical wave length of Bénard cells corresponding to a transversal wave number of 3.117 and another wave length corresponding to a transversal wave number of 2.6. With finite B, the confinement introduces the complexity of multiple solutions with various roll numbers. This leads us to find as many as possible the solution branches and to perform linear stability analysis for each solution branch found. This is also one of the challenges of PRB flows in channels of finite transversal extension.

3.4 Onset of wavy instability: nonlinear behavior

The nature of the Hopf bifurcations mentioned above can be revealed by a 3D time-stepping code. The time-stepping code used has been taylored for natural convection flows in a cavity and described in [25]. Periodic conditions are imposed in the x direction and the initial conditions are longitudinal rolls randomly perturbed. A spatial resolution of $30 \times 200 \times 30$ is used and only one Rayleigh number of 3800 is studied for all the three solution branches of longitudinal rolls found above. Other parameters are kept to be the same as above, *ie* $B = 10$, $Pr = 0.71$ and $Re = 200$. The corresponding wave lengths used in the x direction are respectively 7.7 for the branch of 10 longitudinal rolls, 7.4 for the branch of 9 longitudinal rolls and 8.0 for the branch of 11 longitudinal rolls. They correspond to respectively wave numbers of 0.816, 0.849 and 0.785 which are approximately the critical wave numbers.

Figure 11 displays the time evolution of transversal v velocity at $(y, z) = (B/2, 0.25)$ obtained for the solution branch of 10 Bénard cells. As the base solution possesses the reflection symmetry in y, the pointwise v velocity represents the perturbations and indicates the breaking of reflection symmetry in y: we distinguish an early linear phase with exponential growth in time and a final saturated phase of periodic solution with constant amplitude. Log-scale of the perturbation amplitude shows that the Hopf bifurcation is supercritical. As depicted by Figure 12, instantaneous flow displays wavy structure which is convected downstream. Similar results are obtained for the other two branches of longitudinal rolls and the corresponding details can be found in Figures 13, 14, 15 and 16. Note that steady-state solutions of 9 and 11 Bénard rolls are centro-symmetric and that the base temperature at the channel center is equal to 0.5. Figures 13 and 15 show that the centro-symmetry of the base flows is broken and that the Hopf bifurcations are supercritical.

4 Concluding remarks

Although in the literature there are many recent experimental works on longitudinal rolls of Poiseuille-Rayleigh-Bénard (PRB) flows (see [6, 7, 8, 21] among others), stability analyses of longitudinal rolls of PRB flows in channels of finite transversal extension remain rare. Apart from the work of Kato and Fujimura [13] for a square channel, the present work represents another excursion into stability analyses of longitudinal rolls of PRB flows in channels of finite transversal extension. The methodologies and numerical tools used, time-stepping codes, steady-state solving and continuation method, have been developed for natural convection flows in cavities and they were found to be very efficient for PRB flows in channels of finite transversal extension.

An air-filled channel of transversal aspect ratio of 10 is chosen and Reynolds number is fixed at 200. We first studied the onset of longitudinal rolls, the four most unstable linear modes and the corresponding critical Rayleigh numbers were calculated. The first two modes, Modes 1 and 2, contains Bénard cells of almost equal size and are regular while the other two are irregular. Nonlinear studies using a 2D time-stepping code showed that Modes 1 and 2 lead to supercritical pitchfork bifurcations and that, at some appropriate Rayleigh numbers, Mode 3 leads to an isolated branch of 11 Bénard cells with a turning point at $Ra = 2120$. We found in total three solution branches of stable steady-state longitudinal rolls. The questions which remain to be answered are whether there are other solution branches and why the irregular modes do not result in similar nonlinear solutions.

Linear stability analysis of the three solution branches of longitudinal rolls was performed with respect to 3D periodic perturbations. Similar to longitudinal rolls in a channel of infinite transversal extension [9] and in a square channel [13], they become unstable to 3D wavy oscillatory perturbations. Neutral curves and critical angular frequency were computed by using continuation method. Compared to [9], the lateral confinement of the channel gives the neutral curves a more usual form although it keeps the linear relationship between angular frequency and wave number. Nonlinear studies using a 3D time-stepping code showed that unstable oscillatory linear modes results in supercritical Hopf bifurcations. It is clear that the present work concerns only $B = 10$, $Pr = 0.71$ and $Re = 200$ and that further studies are needed for different values of B, Pr and Re. The fact that there are multiple solutions of longitudinal rolls at large B complicates very much this type of studies as the number of possible branches is unknown. Clever and Busse [9] showed that, at small Reynolds number (with weak Poiseuille flow) in a channel of infinite transversal extension, there are, at higher Rayleigh numbers, oscillatory instabilities arising purely from Bénard rolls and that the corresponding eigen-values are distinguished from those leading to wavy instabilities which are termed sometimes as wavy oscillatory instatiblities in the present paper. It will be interesting to investigate,

in the future, oscillatory instabilities at small Reynolds number in a channel of finite transversal extension as was done for a square channel by Kato and Fujimura [13].

Note that, although it is common for rotating axisymmetric 2D flows to have three non-trivial velocity components, it is rare for 2D flows in Cartesian coordinates to possess this property. Longitudinal rolls of PRB flows in the vertical $y-z$ plane do have this property and stability of longitudinal rolls is the most complicated configuration for linear stability analysis in Cartesian coordinates due to the fact that the 2D base flows possessing three non-trivial velocity components couples the real and imaginary parts of perturbations. It is also of pratical interest to perform this type of linear stability analysis and show the feasibility.

Acknowledgement: computations have been performed on NEC-SX5 supercomputers at IDRIS (Orsay, France) under research project 41474.

References

[1] D. Avsec. Sur les formes ondulées des tourbillons en bandes longitudinales. *C. R. Acad. Sci., Ser. II b*, 204:167–169, 1937.

[2] D. Avsec and M. Luntz. Tourbillons thermoconvectifs et électroconvectifs. *La météorologie*, 31:180–194, 1937.

[3] C. Bernardi and Y. Maday. Approximations spectrales de problèmes aux limites elliptiques. In *Collection Mathématiques & Applications*. Springer Verlag, 1992.

[4] C. Canuto, M.Y. Hussaini, A. Quarteroni, and T.A. Zang. *Spectral methods in fluid dynamics*. Springer Verlag, New York, 1988.

[5] P. Carrière and P. A. Monkewitz. Convective versus absolute instability in mixed Rayleigh-Bénard-Poiseuille convection. *J. Fluid Mech.*, 384:243–262, 1999.

[6] M. Y. Chang and T. F. Lin. Experimental study of aspect ratio effects on longitudinal vortex flow in mixed convection of air in a horizontal rectangular duct. *Int. J. Heat Mass Trans.*, 41:719–733, 1998.

[7] K. C. Chiu, J. Ouazzani, and F. Rosenberger. Mixed convection between horizontal plates -2. Fully developed flow. *Int. J. Heat Mass Trans.*, 30:1655–1662, 1987.

[8] K.C. Chiu and F. Rosenberger. Mixed convection between horizontal plates -1. Entrance effects. *Int. J. Heat Mass Trans.*, 30:1645–1654, 1987.

[9] R.M. Clever and F.H. Busse. Instability of longitudinal rolls in the presence of Poiseuille flow. *J. Fluid Mech.*, 229:517–529, 1991.

[10] K. S. Gage and W. H. Reid. The stability of thermally stratified plane Poiseuille flow. *J. Fluid Mech.*, 33:21–32, 1968.

[11] K.F. Jensen, E.O. Einset, and D.I. Fotiadis. Flow phenomena in chemical vapor deposition of thin films. *Annu. Rev. Fluid Mech.*, 23:197–233, 1991.

[12] Y Kato and K. Fujimura. Prediction of pattern selection due to an interaction between longitudinal rolls and transversal modes in a flow through a rectangular channel heated from below. *Phys. Rev. E*, 62:601–611, 2000.

[13] Y Kato and K. Fujimura. Prediction of three-dimensional breakdown of a longitudinal roll in a square duct. In *The 50th Japan Nat. Congress on Theoretical and Applied Mechanics*, volume 50, pages 327–333, Japan, 2001.

[14] H. B. Keller. Numerical solution of bifurcation and nonlinear eigenvalue problems. In P. H. Rabinowitz, editor, *Applications of Bifurcation Theory*, pages 359–384. Academic Press, 1977.

[15] J. M. Luijkx. *Influence de la présence de parois latérales sur l'apparition de la convection libre, forcée et mixte.* PhD thesis, Université d'état de Mons, 1983.

[16] R. L. Mahajan. Transport phenomena in chemical vapor deposition systems. *Adv. Heat Trans.*, 28:339–415, 1996.

[17] C.K. Mamun and L.S. Tuckerman. Asymmetry and Hopf bifurcation in spherical Couette flow. *Phys. Fluids*, 7(1):80–91, 1995.

[18] H. W. Müller, M. Lücke, and M. Kamps. Transversal convection patterns in horizontal shear flow. *Phys. Rev. A*, 45:3714–3725, 1992.

[19] X. Nicolas. Revue bibliographique sur les écoulements de Poiseuille-Rayleigh-Bénard : écoulements de convection mixte en conduites rectangulaires horizontales chauffées par le bas. *Int. J. of Therm. Sci.*, 41:961–1016, 2002.

[20] X. Nicolas, J.M. Luijkx, and J.K. Platten. Linear stability of mixed convection flows in horizontal rectangular channels of finite transversal extension heated from below. *Int. J. Heat Mass Trans.*, 43:589–610, 2000.

[21] M.T. Ouazzani, J.K. Platten, and A. Mojtabi. Etude expérimentale de la convection mixte entre deux plans horizontaux à températures différentes—2. *Int. J. Heat Mass Trans.*, 33:1417–1427, 1990.

[22] J. Shahda and U. Narusawa. On pattern selection in mixed convection in rectangular ducts. *Heat & Mass Transfer*, 32:213–222, 1997.

[23] L.S. Tuckerman and D. Barkley. Bifurcation analysis for timesteppers. In *Numerical Methods for Bifurcation Problems and Large-Scale Dynamical Systems*, volume 119, pages 453–466. Springer, Bologna, 2000.

[24] S. Xin and P. Le Quéré. Linear stability analyses of natural convection flows in a differentially heated square cavity with conducting horizontal walls. *Phys. Fluids*, 13(9):2529–2542, 2001.

[25] S. Xin and P. Le Quéré. An extended Chebyshev pseudo-spectral benchmark for the 8:1 differentially heated cavity. *Int. J. Num. Meth. in Fluids*, 40(8):981–998, 2002.

[26] S. Xin, P. Le Quéré, and O. Daube. Natural convection in a differentially heated horizontal cylinder : Effects of Prandtl number on flow structure and instability. *Phys. Fluids*, 9(4):1014–1033, 1997.

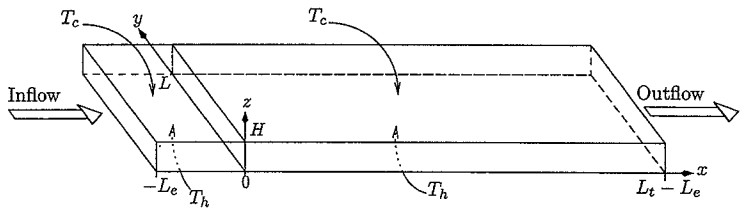

Figure 1: Illustration of Poiseuille-Rayleigh-Bénard flows in a horizontal channel. A pressure driven air flow comes into the channel of aspect ratio $B = L/H$ at $x = -L_e$ and exits at $x = L_t - L_e$. The channel is heated at a constant temperature T_h through the bottom wall and cooled at a constant temperature T_c through the top wall. With very large L_e and L_t, the onset of longitudinal rolls in the channel of infinite length can be studied in the 2D vertical $(y-z)$ plane at $x = 0$.

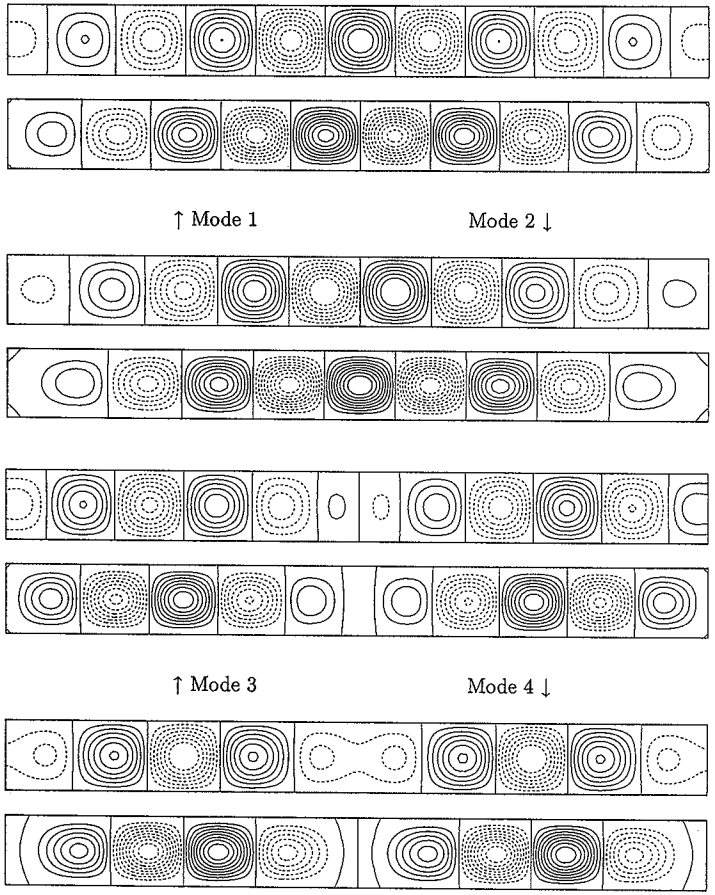

Figure 2: Linear unstable modes (for each mode, eigen-temperature θ is on top and eigen-stream function is at bottom) responsable for the onset of longitudinal rolls of PRB air flows in a channel of transversal aspect ration $B = 10$. Modes 1 and 2 containing respectively 10 and 9 Bénard cells are regular modes in the sense that the Bénard cells are of almost equal size while Modes 3 and 4 are irregular modes.

	Ra_c	Number of rolls	Spatial resolution
	$B = 3$		
present work	1870.5833	3	60×20
Nicolas *et al* [20]	1870.72	3	8×8
Kato and Fujimura [12]	1870.58	3	33×33
	$B = 4$		
present work	1810.2690	4	60×20
	1810.2690	4	80×20
Nicolas *et al* [20]	1810.48	4	8×8
Luijkx [15]	1810.285	4	14×6
Kato and Fujimura [12]	1810.27	4	33×33

Table 1: Critical Rayleigh numbers corresponding to the onset of longitudinal rolls for $B = 3$ and 4.

	Ra_c	Number of rolls	Symmetry
Mode 1	1728.833	10	Reflection in y
Mode 2	1732.433	9	Centro-symmetry
Mode 3	1791.438	11	Centro-symmetry
Mode 4	1811.529	12	Reflection in y

Table 2: Critical Rayleigh numbers corresponding to the onset of longitudinal rolls obtained for $B = 10$ with a spatial resolution 140×30. The same results are also confirmed by a higher spatial resolution of 200×30.

Base solution (Number of rolls)	k_c	ω_c	Ra_c
10	0.818 ± 0.001	0.83103	3414.62 ± 0.03
9	0.859 ± 0.001	0.87183	3663.72 ± 0.03
11	0.784 ± 0.001	0.79791	3231.30 ± 0.03

Table 3: Critical wave number, angular frequency and Rayleigh number with respect to 3D oscillatory perturbations obtained for different branches of base solutions with a spatial resolution of 200×30.

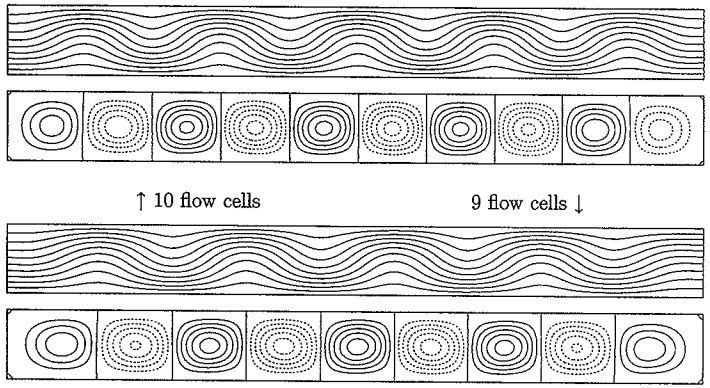

Figure 3: Steady-state solutions (temperature on top and stream function at bottom) resulted from respectively the linear unstable Modes 1 and 2 for $B = 10$, $Pr = 0.71$, $Ra = 2000$ and $Re = 200$. Both the time evolutions of perturbations and final flow structures, similar to the linear unstable modes, indicate that the corresponding bifurcations are supercritical.

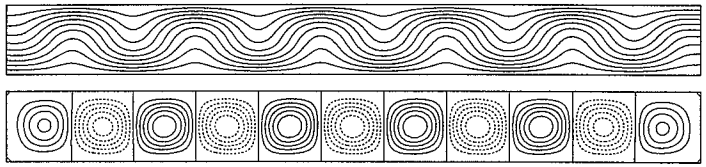

Stable steady-state solution at $Ra = 2400$ on the upper branch.

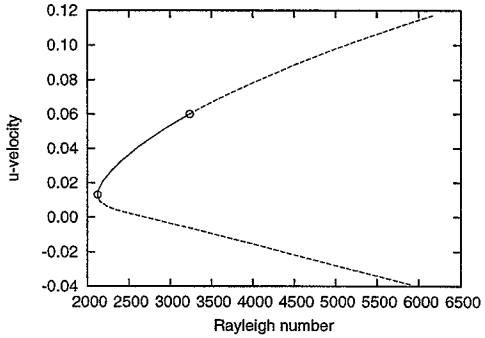

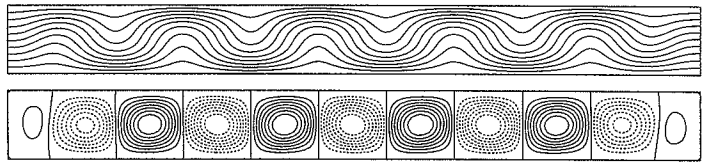

Unstable steady-state solution at $Ra = 2500$ on the lower branch.

Figure 4: Diagram of solutions with 11 Bénard cells for $B = 10$, $Pr = 0.71$ and $Re = 200$. A stable solution with 11 regular cells is first obtained at $Ra = 2400$ (top) by using the base solution perturbed by Mode 3. It is followed for higher and lower Rayleigh numbers using steady-state solving. The turning point is located at $Ra = 2120$ and quadratic extrapolation allows to go through it and construct the lower unstable branch. The unstable solution at $Ra = 2500$ is shown and the two cells at the channel lateral ends are weakened while other central cells are strengthened. The upper stable branch becomes unstable to 3D oscillatory perturbations leading to wavy oscillatory instability and the critical point is located at $Ra = 3231.30$.

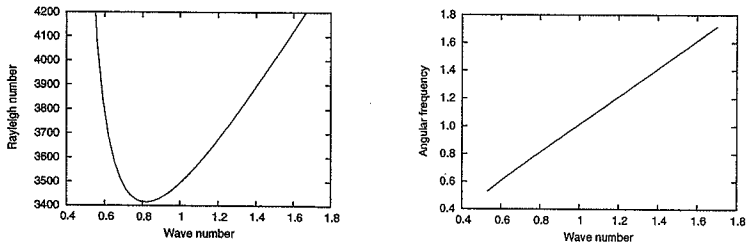

Figure 5: Neutral curve (left) and critical angular frequency (right) obtained for the solution branch of 10 longitudinal rolls with $Pr = 0.71$ and $Re = 200$. The critical angular frequency is linear with the wave number k ($\omega_c = 1.01k$).

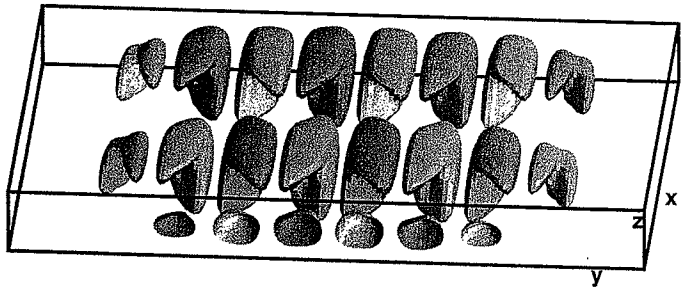

Figure 6: Iso-surfaces of eigen-temperature θ at the critical point (solution branch of 10 longitudinal rolls). The critical mode is strongly damped by the channel lateral confinement and it breaks both the translation symmetry in x and the reflection symmetry in y.

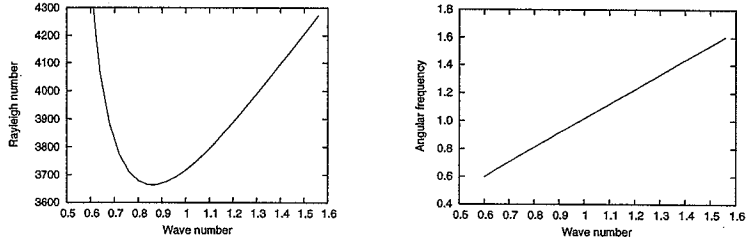

Figure 7: Neutral curve (left) and critical angular frequency (right) obtained for the solution branch of 9 longitudinal rolls with $Pr = 0.71$ and $Re = 200$. The critical angular frequency is linear with the wave number k ($\omega_c = 1.04k - 0.02$).

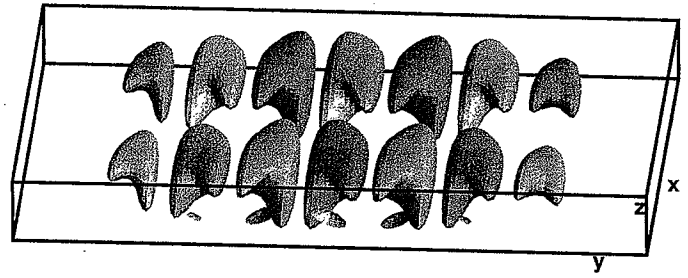

Figure 8: Iso-surfaces of eigen-temperature *theta* at the critical point (solution branch of 9 longitudinal rolls). The critical mode is strongly damped by the channel lateral confinement and it breaks both the translation symmetry in x and the centro-symmetry in $y-z$ plane.

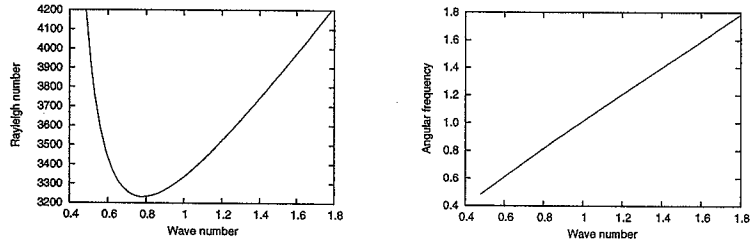

Figure 9: Neutral curve (left) and critical angular frequency (right) obtained for the solution branch of 11 longitudinal rolls with $Pr = 0.71$ and $Re = 200$. The critical angular frequency is linear with the wave number k ($\omega_c = 0.98k + 0.02$).

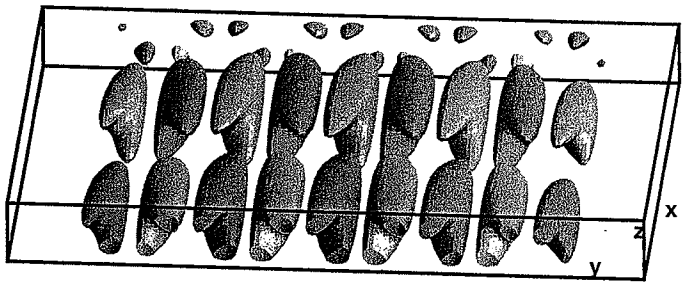

Figure 10: Iso-surfaces of eigen-temperature θ at the critical point (solution branch of 11 longitudinal rolls). The critical mode is strongly damped by the channel lateral confinement and it breaks both the translation symmetry in x and the centro-symmetry in $y-z$ plane.

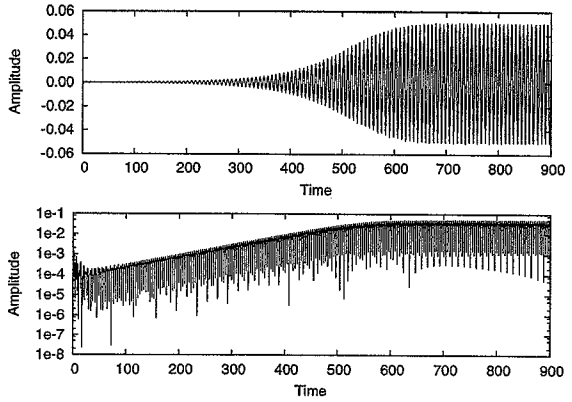

Figure 11: Time trace of transversal velocity at $(y, z) = (B/2, 0.25)$ obtained at $Ra = 3800$ for the solution branch of 10 longitudinal rolls. Perturbations are amplified in time to give rise to a periodic solution. Log-scale of perturbation amplitude shows that the Hopf bifurcation is supercritical.

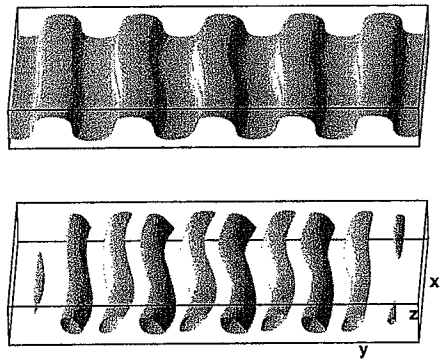

Figure 12: Iso-surfaces of instantaneous temperature (top) and longitudinal velocity (bottom) fields obtained at $Ra = 3800$ for the solution branch of 10 longitudinal rolls. Spatial oscillations of the iso-surfaces illustrates the wavy oscillatory instability of longitudinal rolls. One should imagine that these spatial oscillations are travelling downstream in time.

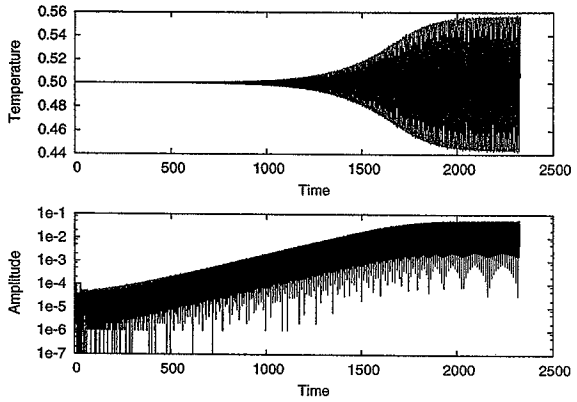

Figure 13: Time trace of transversal velocity at $(y, z) = (B/2, 0.5)$ obtained at $Ra = 3800$ for the solution branch of 9 longitudinal rolls. Perturbations are amplified in time to give rise to a periodic solution. Log-scale of perturbation amplitude shows that the Hopf bifurcation is supercritical.

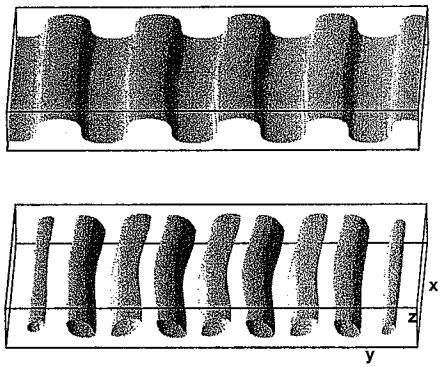

Figure 14: Iso-surfaces of instantaneous temperature (top) and longitudinal velocity (bottom) fields obtained at $Ra = 3800$ for the solution branch of 9 longitudinal rolls. Spatial oscillations of the iso-surfaces illustrates the wavy oscillatory instability of longitudinal rolls.

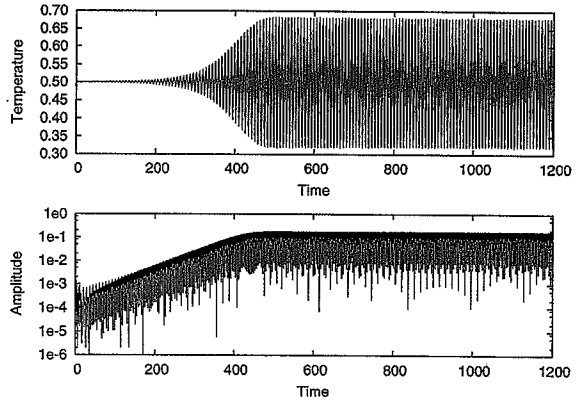

Figure 15: Time trace of transversal velocity at $(y, z) = (B/2, 0.5)$ obtained at $Ra = 3800$ for the solution branch of 11 longitudinal rolls. Perturbations are amplified in time to give rise to a periodic solution. Log-scale of perturbation amplitude shows that the Hopf bifurcation is supercritical.

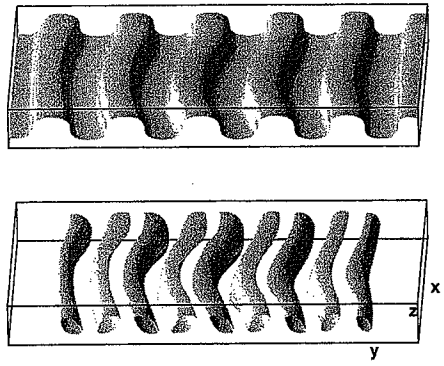

Figure 16: Iso-surfaces of instantaneous temperature (top) and longitudinal velocity (bottom) fields obtained at $Ra = 3800$ for the solution branch of 11 longitudinal rolls. Spatial oscillations of the iso-surfaces illustrates the wavy oscillatory instability of longitudinal rolls. One should imagine that these spatial oscillations are travelling downstream in time.